Short-Range Electron Correlation Stabilizes Noncavity Solvation of the Hydrated Electron

William J. Glover[*,†,‡] and Benjamin J. Schwartz[*,§]

†NYU-ECNU Center for Computational Chemistry, New York University Shanghai, Shanghai, 200122, China
‡Department of Chemistry, New York University, New York, New York 10003, United States
§Department of Chemistry and Biochemistry, University of California, Los Angeles, Los Angeles, California 90095, United States

Ⓢ *Supporting Information*
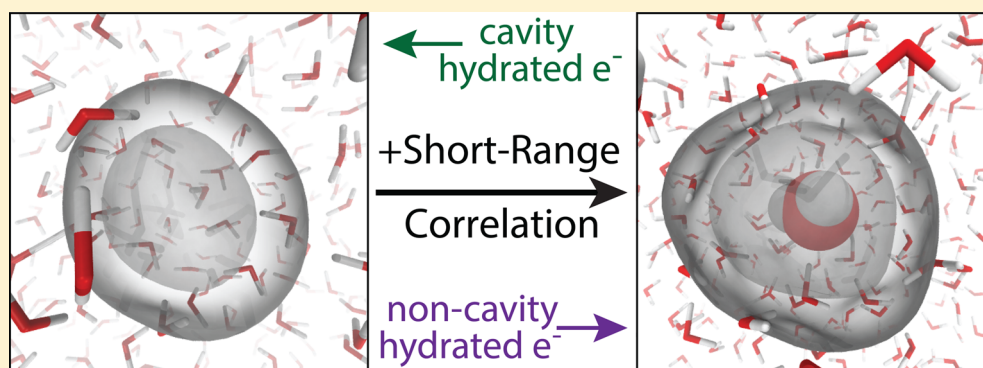
ABSTRACT: The hydrated electron, $e^-_{(aq)}$, has often served as a model system to understand the influence of condensed-phase environments on electronic structure and dynamics. Despite over 50 years of study, however, the basic structure of $e^-_{(aq)}$ is still the subject of controversy. In particular, the structure of $e^-_{(aq)}$ was long assumed to be an electron localized within a solvent cavity, in a manner similar to halide solvation. Recently, however, we suggested that $e^-_{(aq)}$ occupies a region of enhanced water density with little or no discernible cavity. The potential we developed was only subtly different from those that give rise to a cavity solvation motif, which suggests that the driving forces for noncavity solvation involve subtle electron-water attractive interactions at close distances. This leads to the question of how dispersion interactions are treated in simulations of the hydrated electron. Most dispersion potentials are *ad hoc* or are not designed to account for the type of close-contact electron-water overlap that might occur in the condensed phase, and where short-range dynamic electron correlation is important. To address this, in this paper we develop a procedure to calculate the potential energy surface between a single water molecule and an excess electron with high-level CCSD(T) electronic structure theory. By decomposing the electron-water potential into its constituent energetic contributions, we find that short-range electron correlation provides an attraction of comparable magnitude to the mean-field interactions between the electron and water. Furthermore, we find that by reoptimizing a popular cavity-forming one-electron model potential to better capture these attractive short-range interactions, the enhanced description of correlation predicts a noncavity $e^-_{(aq)}$ with calculated properties in better agreement with experiment. Although much attention has been placed on the importance of long-range dispersion interactions in water cluster anions, our study reveals that largely unexplored *short-range* correlation effects are crucial in dictating the solvation structure of the condensed-phase hydrated electron.

1. INTRODUCTION

The nature of the hydrated electron, which is an excess electron embedded in liquid water, continues to be a source of much debate. The consensus view until fairly recently was that the electron locally expels the water and primarily occupies a cavity; both one-electron mixed quantum/classical simulations[1,2] and low-temperature electron paramagnetic resonance (EPR) experiments on alkaline aqueous glasses[3] supported a cavity picture in which the first-shell waters surrounding the hydrated electron point their OH bonds toward the electron's center of mass, in a manner similar to halide solvation.[4,5] Recently, however, our group challenged the cavity picture of the electron, and based on mixed quantum/classical simulations

with a rigorously derived electron-water interaction potential, we suggested that the hydrated electron occupies a region of enhanced water density with little to no appreciable central cavity.[6] This noncavity picture has come to be referred to as the LGS model,[7−9] but we also have labeled it the "inverse plum pudding" picture of the excess electron since several water molecules are embedded inside the electron's wave function.[10] All-electron calculations based on QM/MM density functional theory (DFT) also paint a picture in which there is significant overlap of the excess electron's wave function with the

surrounding water, albeit with a small central cavity.[11] More recently, a zero-Kelvin 4-water cluster continuum solvent model of the hydrated electron was put forward that largely supports the QM/MM DFT picture.[12] With some exceptions, such as the vertical binding energy and the molar solvation volume,[8,9,13−15] the predictions of the noncavity model, however, have been shown to agree with numerous experimental properties of the hydrated electron, in particular the behavior of the hydrated electron at the air/water interface,[15] and the resonance Raman spectrum and temperature-dependent red-shift of the electronic absorption spectrum,[16] none of which are well-described by the more traditional cavity model.

Despite the fact that a noncavity picture of the hydrated electron with significant overlap with nearby water molecules correctly predicts numerous properties, such a picture is still not well accepted. One reason for this is that our basic physical intuition suggests that a closed-shell water molecule should strongly repel an excess electron at close range due to Pauli's exclusion principle. This expectation of Pauli repulsion, combined with a 30-year history of cavity models for describing the hydrated electron,[1,2,17−25] makes a noncavity picture appear somewhat unpalatable. It is worth noting, however, that when one builds an electron-water interaction potential based on Pauli's principle (i.e., constructs a potential that guarantees orthogonality between the excess electron's wave function and that of the wave functions of the electrons in the occupied water molecular orbitals),[26] the repulsive interactions are localized only to where the closed-shell water electron density is appreciable. Moreover, this type of calculation shows clearly that there are regions close to the water molecule (within 1 Å) where there is a net attraction of the excess electron to a nearby water molecule.[6] However, such attractions are likely over-estimated in the LGS model,[7] and clearly additional work is needed to explore how to design one-electron models that accurately capture electron-water interactions.

Of course, none of the above discussion addresses electron correlation, which constitutes an additional source of attraction between an excess electron and a water molecule. At large electron-water separations, the electron-water correlations correspond to dispersion interactions, which are expected to increase with the amount of overlap between the electron and water molecules,[27] and at small electron-water separations, they are better thought of as dynamic electron correlations. Although the importance of dispersion in the energetics of small water anion clusters is well-known,[22,27−32] the influence of dispersion interactions and short-ranged electron correlation on the structure of the bulk hydrated electron has not yet been explored in any depth and is the subject of this paper. The goal of this paper is therefore not to revisit the LGS noncavity model but rather to explore electron-water correlation interactions from first-principles quantum chemistry and to compare these to approximate treatments from one-electron models.

A major challenge associated with exploring dispersion interactions for the bulk hydrated electron is that first-principles quantum chemistry methods that correctly capture this interaction have a computational cost that scales steeply with the number of treated atoms. This has limited the application of second-order Møller−Plesset (MP2)[33] and Coupled-Cluster Singles and Doubles with perturbative triples (CCSD(T))[34] calculations to water clusters of at most a few tens of molecules in size, which is at least an order of magnitude smaller than the

number of water molecules needed to describe the bulk hydrated electron.[6] Furthermore, the electron binding motifs seen in small water clusters are not necessarily representative of the solvation of the bulk hydrated electron due to the former's smaller binding energies. This is because in small water clusters (even those where the electron is localized to the cluster interior), the center of mass of the excess electron is typically located several angstroms away from the water molecules. This means that previous studies of dispersion interactions in these systems explored only long-range electron-water interactions, rather than short-ranged electron correlation, which should play a much larger role in the condensed environment of the bulk hydrated electron.

To allow a high-level quantum chemistry determination of both short-range and long-range electron correlation, in this paper we develop a new procedure to restrain an excess electron at varying desired distances from a single water molecule. Using calculations at the CCSD(T) level, we find that, perhaps not surprisingly, attractive correlation interactions are greatest when an excess electron is restrained to be directly on top of a water molecule, a motif not seen in clusters but one that should play an important role in bulk solution. We then use our calculations to create a pairwise-additive polarization potential that reproduces the distance-dependent CCSD(T) calculations. We find that the resulting polarization-correlation interaction is nearly an order of magnitude larger than assumed in previous calculations.[2] When we then graft this new polarization potential on to a standard cavity-forming one-electron core potential,[2] we find that our improved treatment of correlation gives rise to a noncavity hydrated electron when implemented in a mixed quantum/classical simulation. Overall, our results show that a better treatment of electron correlation dramatically increases the attractive interactions between excess electrons and water molecules over what has been previously thought and greatly strengthens the case for a noncavity structure of the hydrated electron.

2. METHODS

2.1. Using Confining Potentials To Restrain an Excess Electron. In order to treat an excess electron interacting with a single water molecule as a bound electronic structure problem, we followed the work of others[2,24] and added a polynomial confining potential to the electronic Hamiltonian. Previous work used a confining potential of the form $V^{conf} = 0.5k(x^8 + y^8 + z^8)$.[2,24] With a suitably chosen confining strength, k, this potential restricts an electron to the vicinity of the water molecule, while leaving the occupied water molecular orbitals (MOs) essentially unchanged. However, in addition to confining the electron, for the purpose of understanding the distance dependence of electron correlation interactions, we want to also control the size and location of the electron relative to the water molecule. To this end, we constructed a new confining potential according to

$$V^{conf} = 0.5k(x^8 + y^8) + 0.5k_z z^8 - Cz \tag{1}$$

where z points along the water dipole vector, the origin is at the water center of mass, and C is a constant chosen to form a basin of attraction that localizes the excess electron to one side of the water molecule. It should be noted that the linear Cz term in V^{conf} *will* alter the occupied MOs of water by polarizing them along the water dipole vector. This is intentional on our part, and we make use of this to mimic condensed-phase effects on

the electronic structure of water by choosing $C = 0.015167$ au such that the resulting dipole moment of an isolated water at the Hartree–Fock level becomes equal to that of the SPC water model with the same geometry. This makes the application of a one-electron model with SPC charges more rigorous and avoids the need for rescaling of charges from the gas-phase to the condensed-phase, as has been done in previous models.[2,6]

Perpendicular to the molecular dipole, we set the confining potential strength to $k = 1 \times 10^{-7}$ au, which is the value used in previous studies[2,24] and which corresponds to the strongest possible confinement that does not appreciably affect the occupied water molecular orbitals. Finally, in order to control the average distance between the excess electron and the water molecule, the confining potential along the molecular dipole direction was varied according to $k_z = 1 \times 10^{-7} \times 10^{-i/3}$ au with $i = 0...9$. Figure 1 shows V^{conf} (solid black curves) and the spin-density (dashed red curves) of H_2O^- plotted along the molecular dipole for several values of k_z within the considered range. For $k_z = 1 \times 10^{-7}$ au, the electron is largely confined directly on the water molecule, while for $k_z = 1 \times 10^{-10}$ au, the electron is localized approximately 10 Bohr away from the water. For all confinement strengths, the electron has a spatial extent of fwhm ≈ 5.5 Bohr, comparable to the known fwhm ≈ 4.9 Bohr of the condensed-phase hydrated electron.[35]

It should be noted that our choice of biasing potential localizes the excess electron on the oxygen side of water, as can be seen clearly from Figure 1. Although this may appear unphysical from the point of view of normal aqueous anion solvation (which typically occurs via H-bonding),[4,5] it is worth noting that the hydrated electron does not behave as a typical anion. Its electron density is diffuse (diameter of ~5 Å) and overlaps with a number of nearby water molecules whether it exists in a cavity or not. Thus, the hydrated electron experiences the oxygen side of water about as much as the hydrogen side.[10] Moreover, the short-range correlation interactions we are interested in scale roughly with molecular polarizability and the polarizability of water is largely isotropic,[36] so it should not matter in which direction the electron is biased. To verify this, we will show below that the potential we develop by confining the electron to the oxygen side of water also reproduces high-level quantum chemistry calculations in confining potentials without a linear term where the electron localizes to the hydrogen side of water.

2.2. Basis Set. One challenge associated with performing quantum chemistry calculations in the presence of the confining potential of eq 1 is the very slow convergence of the excess electron's wave function with basis-set size when atom-centered basis functions are used exclusively. The origin of the slow convergence is the presence of a basin of attraction in V^{conf} where the excess electron localizes several Bohr away from the water molecule (see Figure 1) and where coverage and flexibility from atom-centered basis functions is poor, even if diffuse functions are used. To overcome the limitations of atom-centered bases, we used a $7 \times 7 \times 13$ regular rectangular grid of spherical Gaussians in combination with the standard aug-cc-pVTZ basis. The Gaussian Grid (GG) functions were separated by 2.5 bohr, and the grid origin was the water center-of-mass. Each GG function had an exponent of 0.16 au. We carefully chose these values to ensure convergence of the eigenvalue of a single electron in the confining potential to within 0.01 eV of the numerically exact value across the entire range of confinement strengths.
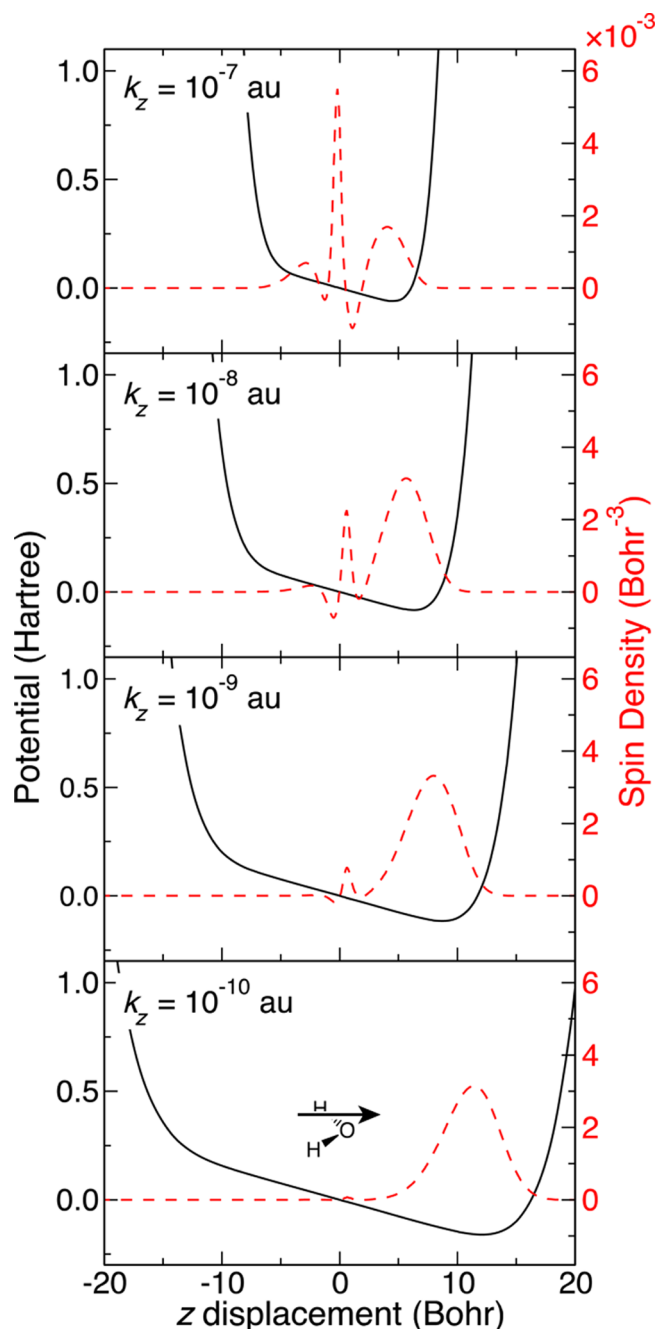

Figure 1. Confining potentials (solid black curves, left axis) for four different dipole axis confinement strengths and the corresponding spin density (dashed red curves, right axis) of H_2O^- calculated at the UHF/aug-cc-pVTZ+PGG level (see text for basis set definition). To avoid sharp features at the oxygen atomic core, we plot the spin density along the water dipole but displaced 0.5 Bohr above the molecular plane (indicated by the molecular drawing in the bottom panel).

The combined basis of aug-cc-pVTZ and the GG functions is a set of 742 functions, which unfortunately was too large for CCSD(T) calculations with our available computational resources. A reduction in the number of GG functions is possible, however, since roughly half of the GGs are located in regions of high potential (e.g., at negative values of z) and therefore do not contribute significantly to the excess electron's wave function. We therefore constructed a Pruned Gaussian Grid (PGG) by discarding basis functions that had MO coefficients with absolute value less than 0.001 in all of the

UHF occupied orbitals of H_2O^-. By doing this, we compressed the basis to between 337 and 374 functions (depending on the confining strength) while maintaining an error in the MP2 VBE of less than 0.01 eV. The aug-cc-pVTZ+PGG basis set is just small enough to allow CCSD(T) calculations to be performed on this system.

3. RESULTS AND DISCUSSION

3.1. Correlation and Dispersion Effects between Excess Electrons and Water: Many-Electron Quantum Chemistry Calculations. For each confining potential, $k_z = 1 \times 10^{-7} \times 10^{-i/3}$ au; $i = 0...9$, we used Q-Chem 4.3 to perform unrestricted HF, MP2, and CCSD(T)/aug-cc-pVTZ+PGG calculations on both H_2O and H_2O^-,[37] with the neutral geometries optimized at the CCSD(T)/aug-cc-pVTZ level in the absence of the confining potential. For the MP2 and CCSD(T) levels of theory, the Vertical Binding Energy (VBE) was computed from $E(\text{neutral}) - E(\text{anion})$, while the Frozen-Core Hartree−Fock (FCHF) Binding Energy is equal to the negative of the LUMO energy of neutral H_2O (Koopman's theorem).[38] To remove the effects of the confining potential, which dominates the energetics of the electron, we subtracted the VBE of H_2O^- in the confining potential from the VBE of a bare electron in the confining potential to give an effective electron-water interaction energy: $E^{e^- \text{-water}} = \text{VBE}(e^-) - \text{VBE}(H_2O^-)$. Positive values of the electron-water interaction energy correspond to a net repulsion between the electron and water molecule.

We start by considering the FCHF result, otherwise known as the static exchange approximation, since this has formed the basis for constructing most electron-water pseudopotentials to date.[2,6,18,22−24,29] This level of theory captures mean-field Coulomb, Exchange, and Pauli interactions between the excess electron and water molecule but neglects electron correlation effects and polarization of the occupied water orbitals by the excess electron. Figure 2(a) shows the FCHF electron-water interaction energy ($\times$ symbols) for the range of confining potentials discussed in Section 2.1. The interaction energy is seen to be repulsive and monotonically decreases with decreasing confining potential strength (i.e., with increasing electron-water distance). This makes sense given that the confining potential restrains the excess electron to the oxygen side of water, and the electron therefore experiences a net Coulombic repulsion from the water dipole moment.

Next, we consider the electron-water interaction energy at the UHF level (Figure 2(b), $\times$ symbols). Comparing to panel (a), we see the UHF result is in close agreement with the FCHF energies, which follows from Koopman's theorem.[38] The small deviations between UHF and FCHF are a result of orbital relaxations at the UHF level, which are evidently quite modest in this system. Going beyond UHF, we consider next the effects of electron correlation at the MP2 (open circles) and CCSD(T) (+ symbols) levels of theory. Here we see that electron correlation substantially reduces the overall repulsion between the excess electron and water molecule at short-range, by as much as 0.33 eV when the electron is restrained to be essentially on the water molecule at the largest confinement strength. The MP2 and CCSD(T) calculations are in close agreement, indicating that any correlation effects beyond second order in this system are relatively minor. Most interesting is the resulting potential energy curve between the electron and water: when electron correlation is included, the
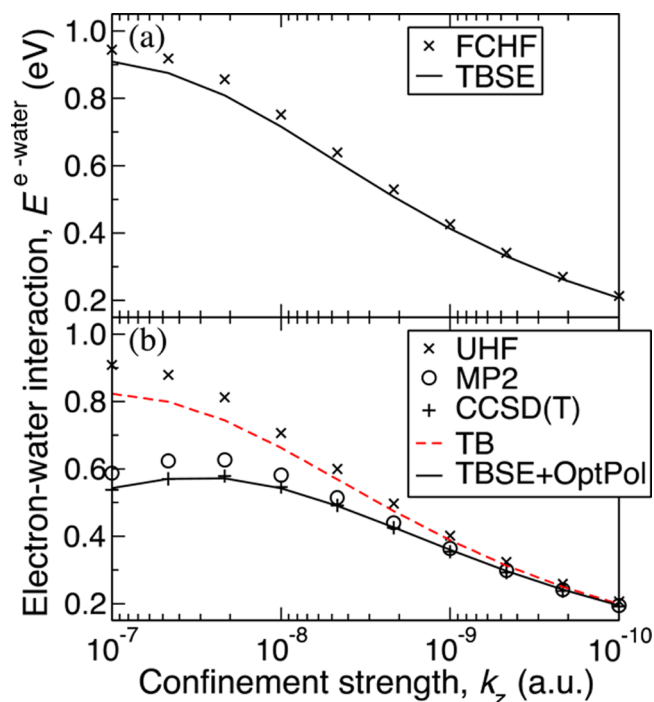

Figure 2. Electron-water interaction energies (see text for definition) over a range of confining potentials. Panel (a): Frozen-Core Hartree−Fock (FCHF, $\times$ symbols), and one-electron Turi-Borgis Static-Exchange core potential (TBSE, solid black curve). Panel (b): The same calculation at the UHF ($\times$ symbols), MP2 (open circles), and CCSD(T) (+ symbols) levels of theory. Also shown are one-electron TBSE with the original added TB polarization potential (TB, dashed red curve) or the TBSE core potential with an added polarization potential optimized to fit our calculated CCSD(T) interaction energies (TBSE+OptPol, solid black curve). The dip in the CCSD(T) interaction energies for the highest confinement strengths indicates that short-range electron correlation is important in stabilizing an excess electron confined to the immediate vicinity of a water molecule.

potential curve is relatively flat in the vicinity of the water molecule and even exhibits a local minimum when the electron is directly on the water molecule, suggesting that due to a balance of correlation-based attractive and static exchange-based repulsive interactions, there are no net strongly repulsive forces between the electron and water at short-range.

To better understand the attractive interactions between the electron and water, the effects of correlation on the interaction energy can be quantified by the excess-electron correlation energy[30]

$$\Delta = E_{\text{corr}}(\text{anion}) - E_{\text{corr}}(\text{neutral}) \tag{2}$$

where E_{corr} is the correlation energy, defined at the MP2 level as $E_{\text{corr,MP2}}(\text{anion}) = E_{\text{MP2}}(\text{anion}) - E_{\text{UHF}}(\text{anion})$. Since the correlation energy of a single electron system is zero, the excess-electron correlation energy is equal to the difference between electron-water interaction energies at the correlated and UHF levels:

$$\Delta = E_{\text{MP2}}^{e^- \text{-water}} - E_{\text{UHF}}^{e^- \text{-water}} \tag{3}$$

From Figure 2, we see that Δ is negative for all electron-water distances, which means that electron correlation preferentially stabilizes the anion over the neutral species. Furthermore, if one stops at second order and ignores the effects of orbital relaxation (approximations that are both

justified by the results in Figure 2), the excess-electron correlation energy can be written as a sum of Pair Correlation Energies (PCEs) between the excess electron SOMO and the occupied water spin orbitals[27]

$$\Delta \approx \sum_{i \neq SOMO} E_{i,SOMO}^{PCE} \qquad (4)$$

where each PCE is given by

$$E_{i,SOMO}^{PCE} = \sum_{a<b} \frac{|\langle \varphi_i \varphi_{SOMO} || \varphi_a \varphi_b \rangle|^2}{\varepsilon_i + \varepsilon_{SOMO} - \varepsilon_a - \varepsilon_b} \qquad (5)$$

Eq 5 follows standard notation: φ_i is an occupied water spin orbital with corresponding Hartree–Fock eigenvalue ε_i, and φ_a and φ_b are virtual water orbitals. Eqs 4 and 5 are equivalent to the definition of electron-molecule dispersion energies for dipole-bound anions proposed by Gutowski et al.[39] In addition, eq 4 provides a way to separate the correlation interaction into contributions from each water spin orbital based on PCEs involving the SOMO.

The PCEs between the occupied water spin orbitals and the SOMO were computed in a development version of PSI4,[40] and their cumulative sums are shown in Figure 3 as a function
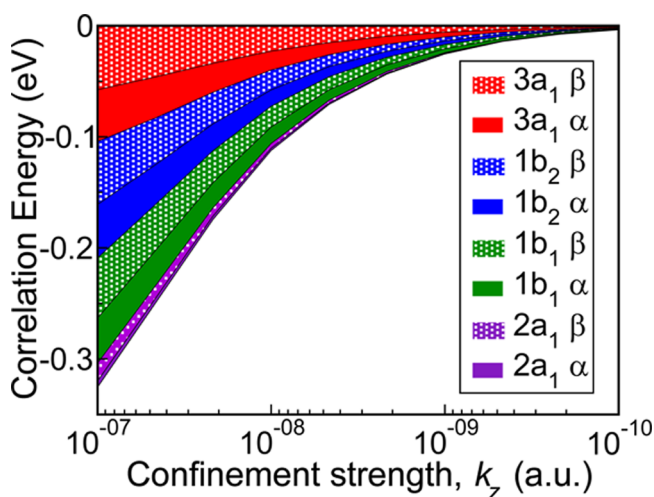

Figure 3. MP2 electron-water Pair Correlation Energies (PCEs) between the SOMO and each occupied water spin orbital (eq 5) over a range of confining potentials, displayed cumulatively from the largest contribution (SOMO:3a$_1\beta$ pair) to the smallest (SOMO:2a$_1\alpha$ pair). Since correlation effects beyond second order are negligible for this system (cf. Figure 2), the sum of the PCEs gives the net electron-water correlation interaction (eq 4). Note: the SOMO:1a$_1$ pair correlation energies are zero since the 1a$_1$ orbital is treated as a frozen core in the MP2 calculations.

of the confining potential strength. The largest PCEs over the entire range of confining potentials involve the 3a$_1$ spin orbitals (red filled segments), with the 1b$_2$ (blue segments) and 1b$_1$ (green segments) showing PCEs of comparable magnitude. The 2a$_1$ PCEs are consistently the smallest in magnitude, and all PCEs are seen to decrease monotonically in magnitude as the confining potential strength is weakened.

This behavior of the PCEs can be understood from eq 5: the largest two-electron repulsion integrals in the numerator occur when the SOMO overlaps strongly with a given occupied water orbital. In particular, the 3a$_1$ spin orbitals have large contributions from the 2p$_z$ atomic orbital of oxygen, which

points toward the SOMO and therefore overlaps the most strongly with it. The 2a$_1$ molecular orbitals, on the other hand, are comprised of the more compact 2s atomic orbital of oxygen; this orbital has a more negative HF eigenvalue, leading to a smaller numerator and larger magnitude denominator than for the 3a$_1$ PCE. Furthermore, at weaker confining potentials, corresponding to larger electron-water separations, the overlap between SOMO and all of the occupied orbitals decreases, leading to a reduction in magnitude of the PCEs. What is quite surprising, however, is the large magnitude of the PCEs at high confining strengths: for $k_z = 10^{-7}$ au, where the excess electron lies essentially on top of the water molecule, the 3a$_1$ PCE is around 0.06 eV. This value is an order of magnitude larger than the PCEs Williams and Herbert calculated for small water anion clusters,[27] which makes sense given that the binding motifs of water anion clusters sample only weaker long-range dispersion interactions, not the short-range electron correlation interactions that are more relevant in the condensed phase.

3.2. The Role of Electron Correlation in One-Electron Pseudopotential Calculations of an Excess Electron Interacting with a Water Molecule.
Having seen that correlation energies at small electron-water separations are comparable in magnitude to the mean-field UHF electron-water interactions (i.e., to the sum of Pauli, Coulomb, and exchange interactions), we turn next to exploring how such high-level quantum mechanical effects might be incorporated into the types of one-electron pseudopotentials that are used in mixed quantum/classical simulations of the hydrated electron. To this end, we decided to compare one-electron model calculations of an excess electron interacting with a single water molecule in the confining potential of eq 1 to the CCSD(T) many-electron calculations discussed above. For this purpose, we have chosen the widely used Turi-Borgis (TB) electron-water potential.[2] Although more advanced electron-water potentials that incorporate many-body polarization have recently been developed,[24,32] the goal of this work is not to develop the "ultimate" electron-water pseudopotential but rather to explore the qualitative effects of a better description of short-range electron correlation in a one-electron model. In this regard, the TB model is particularly suitable as it incorporates electron correlation via a polarization potential with just two parameters, allowing us to change as few variables as possible in the model in order to glean physical insight.

For our calculations, we expanded the excess electron's wave function in a Fourier-Grid basis of $36 \times 36 \times 36$ plane waves spanning a cubic cell of 38.1 Bohr in length. The electron's ground-state energy (equal to its negative binding energy) was found by solving the one-electron eigenvalue problem using the Davidson algorithm.[41]

We begin our examination of the TB potential by seeing how well it describes electron-water interactions other than those arising from electron correlation. Thus, we first performed one-electron calculations using the static-exchange part of the TB potential (TBSE), since this accounts for mean-field Coulomb, Exchange, and Pauli repulsion interactions between the electron and closed-shell water molecule, assuming fixed water orbitals.[2] This level of theory yields an excess electron's wave function that corresponds to a pseudo-LUMO of a closed-shell water molecule[18,26,42] and therefore provides a clean way to separate out polarization of the water orbitals by the excess electron, which can be treated with an added polarization potential (see below). Although the TBSE model uses atom-centered partial charges from the SPC model, the electron in this model does

not see point charges; instead, the partial charges are modeled as Gaussian charge distributions, which therefore include higher-order multipole interactions implicitly.

The electron-water interaction energies with the TBSE pseudopotential are plotted as the solid black curve in Figure 2(a), and these compare very favorably with the many-electron FCHF results, further justifying our use of the TB one-electron model. This agreement is perhaps not surprising since the TBSE potential was constructed to reproduce a FCHF calculation in the standard confining potential.[2] The agreement at short-range is not perfect, however, and this can be traced to our inclusion of the linear Cz term in the confining potential that serves to polarize the occupied water orbitals and increase the molecular dipole moment to match the condensed-phase SPC water model. The TBSE potential was constructed without a linear term in the confining potential, i.e., with unperturbed gas-phase water orbitals,[2] resulting in an underestimation of the Pauli repulsion of an electron confined to the oxygen side of the water molecule compared to FCHF results. This reveals that one-electron potentials constructed for gas-phase water molecules are not strictly transferable to the condensed phase, although the nontransferability error seen here is relatively small (≤ 0.03 eV). We note that the transferability error of our LGS core potential,[6] which was tuned to match the dipole of an SPC water and which has been discussed extensively in the literature, is of a comparable magnitude.[7−10]

Given that the TBSE potential adequately describes electron-water interactions at the frozen-core mean-field level, we next consider the inclusion of polarization and electron correlation effects. Although these interactions are many-electron phenomena, their effects, within one-electron model frameworks, are typically incorporated by adding a pairwise polarization potential to the static-exchange core potential that has an asymptotic form of $-\alpha/2r^4$, where r is the radial distance from the water, and α is the isotropic molecular polarizability.[2,18,22,32,43,44] TB chose to use a potential of the form

$$V^{\mathrm{pol}}(r) = -\frac{\alpha}{2(r^2 + R_{\mathrm{c}}^2)^2} \tag{6}$$

where r is the radial distance from the oxygen site of water, $\alpha = 9.7446$ Bohr^3 is the isotropic molecular polarizability of water, and R_{c} is a radial cutoff that prevents a polarization catastrophe at the molecular origin. TB empirically adjusted R_{c} to 4.4 Bohr to reproduce the experimental VBE of the bulk hydrated electron.[2] We performed one-electron calculations using the sum of the TBSE and eq 6 polarization potentials, hereafter donated TB, the results of which are shown as the dashed red curve in Figure 2(b). It is apparent that the TB electron-water interaction energies significantly overestimate both MP2 and CCSD(T) values by as much as ~0.3 eV for small electron-water separations. This means that the polarization potential of eq 6 potential is insufficiently attractive (the fact that there are ~4 first-shell waters in the TB model, 4 quasi-interior waters in more recent multielectron models,[11,13] and over a dozen interior waters in the LGS model[6] could potentially make this per water error comparable to the overall hydrated electron binding energy) and thus a target for improvement.

Having seen that the TB model of polarization inadequately describes electron correlation, we next turn to the question of whether the problem lies with the functional form of eq 6 or TB's choice of parameters. Although one-electron polarization potentials like eq 6 are often described as *ad hoc*,[2,24] it has been

shown previously that the large-distance asymptote of the MP2 correlation potential for an excess electron interacting with a closed-shell species does indeed vary as $-\alpha/2r^4$, assuming the polarizability is isotropic.[44] The correct functional form of the polarization potential at short distances is unfortunately unknown; however, it clearly must be modified from the asymptotic $-\alpha/2r^4$ to avoid a polarization catastrophe at the molecular origin.

To explore the short-range nature of the polarization potential, we assumed isotropic polarizability and kept the functional form of eq 6 while optimizing the parameters α and R_{c} to fit the one-electron model electron-water interaction energies to our reference CCSD(T) energies.[45] We achieved this using the Levenberg−Marquardt algorithm[46] to minimize the square of the deviations between the calculated TBSE plus modified eq 6 electron-water interactions energies and the CCSD(T) values across the range of electron confining potentials. The resulting potential, which we refer to as TBSE+OptPol, has the optimal parameters, $\alpha = 9.25$ Bohr^3 and $R_{\mathrm{c}} = 2.07$ Bohr, and gives electron-water interaction energies (solid black curve in Figure 2(b)) that are in excellent agreement with our CCSD(T) calculations. We also explored whether the Schnitker-Rossky polarization potential,[18] shown as the dot-dashed blue curve in Figure 4, could be optimized to fit the
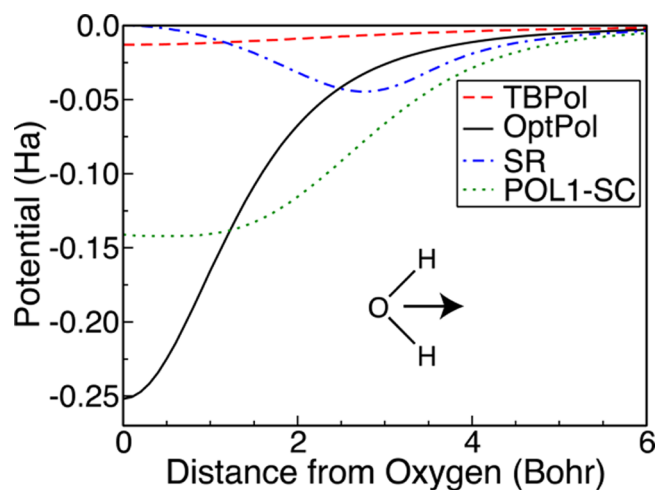

Figure 4. Electron-water polarization potentials. The potential optimized to CCSD(T) energetics (OptPol, solid black curve) is significantly more attractive at short-range than either the original TB polarization potential (TBPol, dashed red curve),[2] the Schnitker-Rossky polarization potential (SR, dot-dashed blue curve),[18] or the POL1-SC polarization potential of Jordan and co-workers (dotted green curve).[32]

CCSD(T) calculations, but we found that the resulting fit was poorer than TBSE+OptPol. Comparing the functional forms of TB and SR polarization potentials suggests that the TB functional form performs better due to its attractive nature at short-range, consistent with the distance dependence of electron correlation demonstrated in Figure 3.

To explore how the polarization potential changes upon optimizing its parameters, in Figure 4 we plot both the original TB polarization potential (TBPol, dashed red curve) and our OptPol potential (solid black curve) along the water molecular dipole with the oxygen atom at the origin. From this figure it is apparent that our new OptPol potential is significantly more attractive than TBPol in the vicinity of the water molecule.

Although the optimized polarizability parameter, α, changed only slightly from TB's original polarization potential to our OptPol, the main difference between the potentials is a result of the much smaller R_c value in OptPol that gives rise to a significant increase in the strength of the potential near the molecular origin.

The extra attraction with our OptPol arises because TB originally chose a value of R_c = 4.4 Bohr empirically to reproduce the experimental VBE of the bulk hydrated electron in a mixed quantum/classical simulation.[2] Since VBEs are very sensitive to long-range polarization, which may have been overestimated in TB's model, it thus appears that by constraining the long-range part of the polarization potential and instead varying R_c to fit the experimental VBE, TB overestimated the damping of the potential at short-range. Indeed, the original TB polarization potential is also significantly weaker than other commonly used electron-water polarization potentials, such as the Schnitker-Rossky model[18] (SR, dot-dashed blue curve in Figure 4) and the POL1-SC polarization potential from the Jordan group[32] (dotted green curve). We note that care should be taken in comparing polarization potentials between different models, however, since the short-range parts of the polarization potential may provide a degree of compensation for deficiencies in the mean-field potential.

Before we apply our TBSE+OptPol potential to the condensed-phase hydrated electron, we return to the question of our assumption of isotropic polarizability: how transferable is our potential beyond that of an electron confined to the oxygen side of a single water molecule's dipole? We explore this by comparing the predictions of our TBSE+OptPol model to CCSD(T) calculations of a single water molecule in a modified confining potential without a linear term:

$$V^{conf} = 0.5k(x^8 + y^8) + 0.5k_z z^8 \qquad (7)$$

The modified confining potential along the water dipole is plotted as the solid black curve in Figure 5, and its influence on an excess electron is shown through the spin density of H_2O^- (solid red curves) for a variety of confining strengths k_z. Comparing to Figure 1, it is clear the absence of a basin of attraction in the confining potential causes the electron to localize mainly on the water molecule and particularly toward the hydrogen side. Without the linear term, decreasing k_z, does not significantly displace the center of the excess electron's charge density away from the water molecule but rather increases the electron's diffuseness. Thus, the confining potential of eq 7 is not as effective as that of eq 1 in biasing an excess electron at varying distances from a water molecule in order to separate short-range interactions from long-range interactions. Nevertheless, quantum chemistry calculations in the confining potential of eq 7 serve as an excellent test of our TBSE+OptPol potential for a type of electron binding that the potential was not explicitly optimized to reproduce. So, we proceed by considering HF, MP2, and CCSD(T) electron-water interaction energies of H_2O^- in the confining potential of eq 7.

The FCHF electron-water interaction energies of H_2O^- in the confining potential of eq 7 are plotted as × symbols in Figure 6(a). It is clear that at the static-exchange level, the water repels the electron, and this repulsion is diminished as the confining potential is weakened and the electron becomes more diffuse. The TBSE potential (dashed blue curve) was designed to reproduce the FCHF result for the $k_z = 10^{-7}$ confining
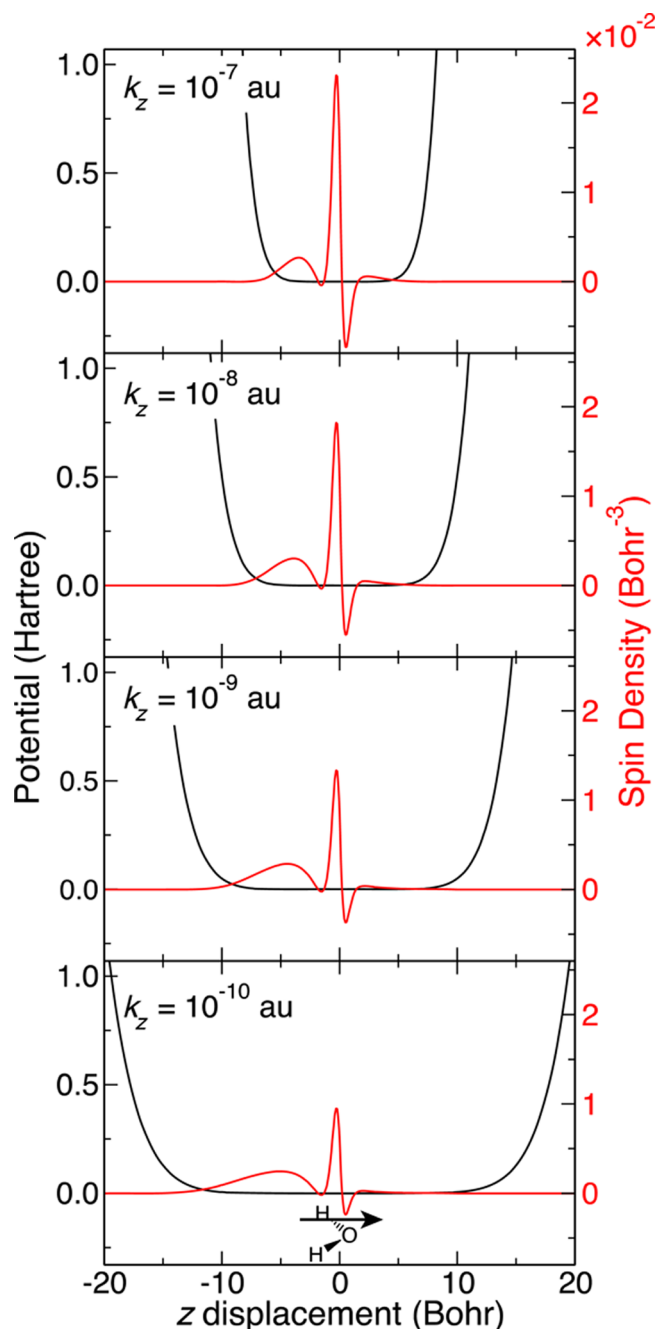

Figure 5. Same as Figure 1, but for confining potentials without a linear term, i.e. eq 7 (solid black curves, left axis). The corresponding spin density (dashed red curves, right axis) of H_2O^- calculated at the UHF/aug-cc-pVTZ+PGG shows that this potential confines the excess electron mainly on the hydrogen side, rather than the oxygen side of the molecule. Unlike confining potentials with a linear term (eq 1), decreasing the degree of confinement only increases the diffuseness of the electron, rather than localizing it significantly away from the water molecule.

potential;[2] however, in this confining potential, the electrostatics of the water molecule correspond to a gas-phase molecule rather than the SPC water model that was used in Figure 2. Therefore, TBSE only agrees with FCHF after scaling the partial charges of the model (which we refer to as TBSE ScQ, solid black curve) to reproduce the gas-phase HF water dipole moment, as was also done in the original construction of the TBSE potential.[20] We thus use scaled partial charges for the
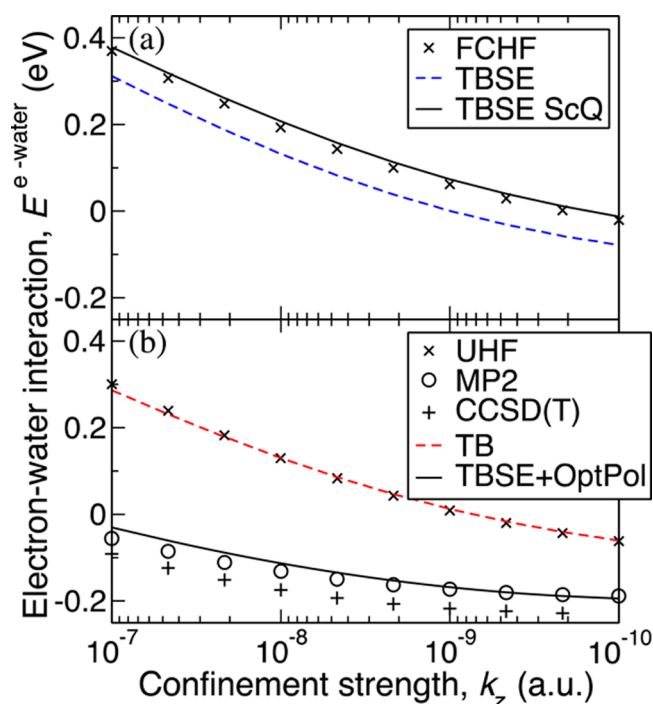
Figure 6. Electron-water interaction energies as in Figure 2 but for confining potentials without a linear term, i.e., eq 7. In panel (a) we see that the one-electron Turi-Borgis Static-Exchange core potential (TBSE, solid black curve) results do not reproduce the Frozen-Core Hartree−Fock (FCHF, × symbols) energies, unless we scale the partial charges on the water molecule to reproduce the HF gas-phase dipole moment of water (TBSE ScQ, dashed blue curve). In panel (b), both the TB (dashed red curve) and TBSE+OptPol (solid black curve) calculations use the scaled partial charges, and we find that TBSE +OptPol performs significantly better than TB at reproducing CCSD(T) energetics (+ symbols). Note: the CCSD(T) data point for $k_z = 10^{-10}$ au is omitted as this calculation was beyond our computational resources because it required a very large PGG basis set.

subsequent TB and TBSE+OptPol calculations in this confining potential.

In panel (b), we consider the effects of going beyond the static exchange approximation. Similar to what is seen in Figure 2(b), the UHF level of theory (× symbols) gives only a modest stabilization over FCHF, indicating that polarization of the water by the excess electron has a small energetic effect. On the other hand, electron correlation at the MP2 and CCSD(T) levels has a much larger effect energetically and actually makes the electron-water interaction attractive at all confining potential strengths. The TB model (dashed red curve) neglects this electron-correlation stabilization and instead captures only UHF-level energetics. The TBSE+OptPol model, however, reproduces the CCSD(T) results quite well: although it overestimates the CCSD(T) energies by ∼0.05 eV, the two potential energy surfaces are largely parallel, and the agreement with MP2 is excellent. We reiterate that TBSE+OptPol was not explicitly fit to reproduce the CCSD(T) energies in this binding motif; however, the good agreement we see verifies that the use of an isotropic polarization potential and the lack of explicit hyperpolarizability in eq 6 is physically reasonable, although it is possible that these two approximations (and lack of many-body polarization) lead to a cancellation of errors. Nevertheless, the good performance of TBSE+OptPol for two very different electron-binding motifs gives us confidence in the trans-

ferability of TBSE+OptPol to model the condensed-phase hydrated electron, which we explore in the next section.

3.3. The Effects of Electron Correlation on the Properties of the Bulk Hydrated Electron. To explore the predictions of our more physically consistent one-electron TBSE+OptPol potential on the properties of the bulk hydrated electron, we performed two Mixed Quantum/Classical (MQC) simulations of a single excess electron and 499 classical SPC/Flex[47] water molecules under periodic boundary conditions. In our first simulation, the electron-water interactions corresponded to the sum of the TB Static Exchange and polarization potentials (i.e., the original TB model) described above, while in our second simulation, we replaced the original TB polarization potential with our optimized version described above in Section 3.2 (TBSE+OptPol). For both simulations, we sampled the Canonical ensemble with Bussi's thermostat[48] at a density of 0.9970479 g cm^{-3} and a temperature of 298 K. The electron was represented in a Fourier-Grid basis of 14 × 14 × 14 plane waves spanning a cubic cell of 29.6 Bohr in length, which was recentered on the electron every 20 fs. At each time step, the lowest electronic eigenvalue was found using Davidson's algorithm.[41] Forces on the water molecules due to the electron were evaluated using the Hellman-Feynman theorem,[49,50] and Born−Oppenheimer Molecular Dynamics was propagated using the velocity Verlet algorithm[51] with a 1 fs time step. Data was sampled from production runs of 4 ns in length after an appropriate equilibration period. We also extended the LGS simulations from ref 6 to a duration of 400 ps in order to have a point of comparison with the results from the TB and TBSE+OptPol simulations summarized in Table 1. Finally, statistical uncertainties in computed expectation values are indicated by 95% confidence limits from the standard error of the sample mean, after subsampling to remove temporal correlations.[52]

3.3.1. Solvation Structure. Figure 7 plots the electron-water Radial Distribution Functions (RDF) for the TB and TBSE +OptPol models. The RDFs for the original TB model (panel a) have been analyzed in detail previously.[2] Briefly, both the electron-hydrogen (solid red curve) and electron-oxygen (dashed red curve) RDFs are zero at the origin and turn on at around 1 and 2 Å, respectively, clearly indicating a solvation motif with a substantial central cavity for the TB model (panel a). Quite remarkably, however, the TBSE+OptPol RDFs (panel b) display noncavity[6] solvation: the electron-hydrogen RDF (dotted black curve) is clearly nonzero at the origin, and the electron-oxygen RDF (dashed blue curve) turns on just inside of 0.5 Å, which is well within the van der Waals radius of water (1.6 Å). A further indication of noncavity solvation is that water molecules are able to penetrate into the center of the excess electron density, and the Table of Contents Graphic shows one such snapshot. This picture is in stark contrast to previous cavity models[2,18,24] and even hybrid models,[11,12] which all have electron-oxygen RDFs that turn on beyond 1.6 Å and do not exhibit water molecules at the center of the excess electron density. Although the solvation shell structure in the TBSE +OptPol model is less well-defined than the original TB model, an inner solvation shell of water is apparent in Figure 7(b), with the first electron-hydrogen peak at a distance of 1.5 Å and an electron-oxygen peak at 2.5 Å. This indicates a slight preference for hydrogen bonds to point in toward the electron's center of mass, despite little or no cavity being present, as is also the case for the LGS noncavity model.[6]
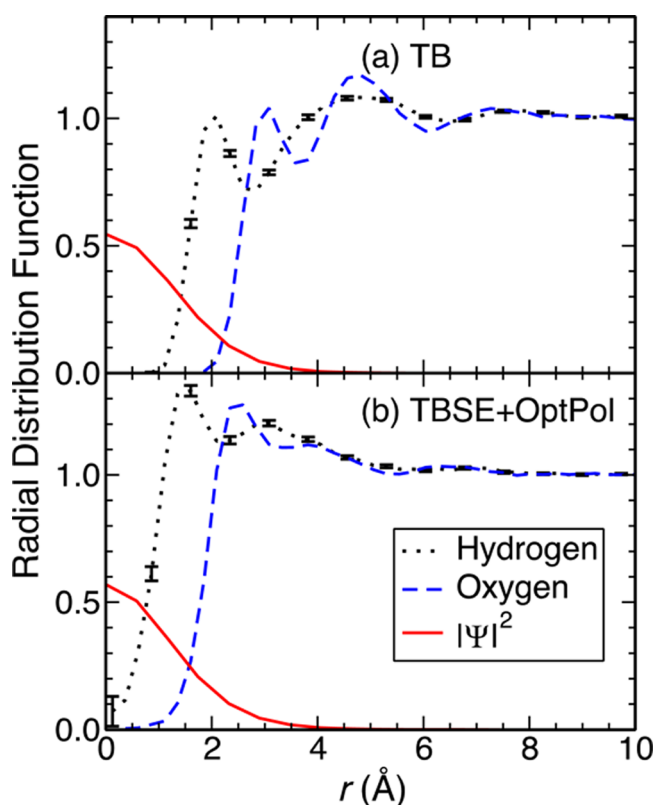
Figure 7. Electron-water radial distribution functions of the bulk hydrated electron computed with the original TB model (panel a) and optimized TBSE+OptPol model (panel b). Also plotted are the averaged radial densities of the electron wave function. Compared to the clear cavity seen with the original TB model, the TBSE+OptPol results show striking noncavity behavior, with a nonzero probability to have a water H atom at the electron's center of mass and significantly more overlap of the electron's charge density with the first-shell waters (cf. Table 1).

Figure 8. Angular distribution of water O−H bonds relative to the O···e⁻ displacement vector computed for the original TB model (panel a) and optimized TBSE+OptPol model (panel b) at varying electron-oxygen distances. Compared to the strong preference for the O−H bond alignment seen with the original TB model, the TBSE+OptPol model's closest waters have a wider range of O−H orientations, consistent with a much less-structured first solvation shell.

We can further analyze the orientations of the first solvation shell molecules by computing the angular distribution function of water O−H bonds relative to the O···e⁻ displacement vector

$$P(\theta) = \frac{\langle \delta(\cos^{-1}(\hat{r}_{OH} \cdot \hat{r}_{O \cdots e^-}) - \theta) \rangle}{4\pi \sin(\theta)} \quad (8)$$

where $\hat{r}_{OH}$ and $\hat{r}_{O \cdots e^-}$ are the O−H bond and O···e⁻ unit vectors, respectively, and the numerator in eq 8 is the unit vector volume element, such that $\int_0^\pi P(\theta) 4\pi \sin(\theta) d\theta = 1$, per O−H bond. The angular distribution of water O−H bonds for the TB model is shown in Figure 8(a) for water oxygens at varying distances r from the electron. Each curve is normalized to be a distribution per water molecule by dividing Eq. 8 by the average number of water molecules at each distance, r. For the water molecules at $r = 3.0 \pm 0.2$ Å and $r = 2.5 \pm 0.2$ Å (dotted black and dashed blue curves, respectively), which correspond to the first-solvation-shell peak of Figure 7(a), the orientation of O−H bonds resembles that seen in halide solvation:[4] one O−H bond is preferentially orientated toward the electron ($\theta \sim 0°$), with the other O−H bond of the same water molecule making an angle of ∼110° with the O···e⁻ vector, as dictated by the H−O−H bond angle of water.

In contrast, Figure 8(b) shows that in the TBSE+OptPol model, the O−H bonds of the first-solvation shell waters take on a much wider range of orientations compared to the TB
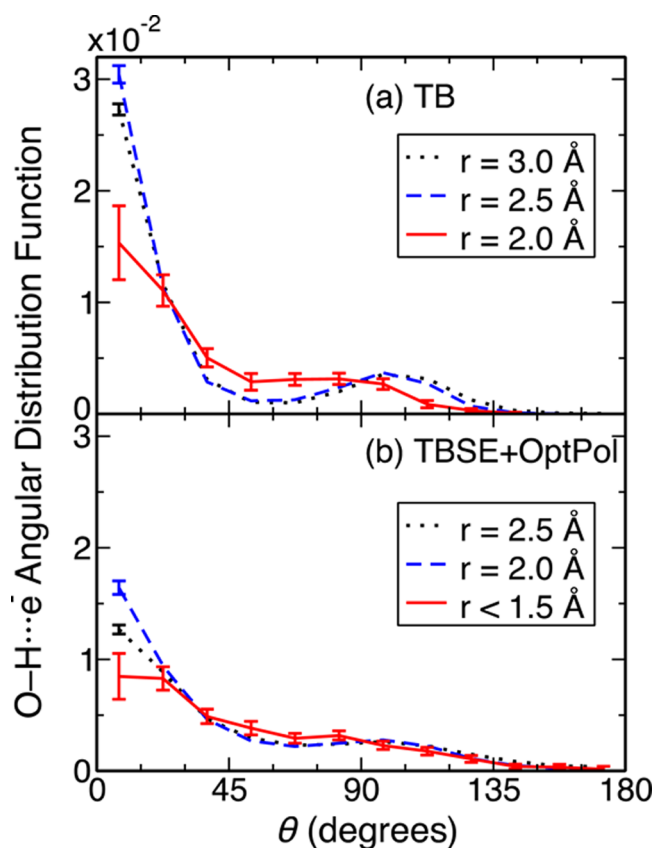
model. This makes physical sense: as the first-solvation shell of the TBSE+OptPol model is compressed inward by ∼0.5 Å relative to the TB model, the increased mutual electrostatic repulsion of the partially positive H atoms of water prevents an ideal O−H-bond aligned solvation motif. Indeed, at the shortest O···e⁻ bond distances in the TB model ($r = 2.0 \pm 0.2$ Å), a similarly increased distribution of O−H bond orientations is seen (Figure 8(a) solid red curve), suggesting that one can think about the structure of TBSE+OptPol as similar to TB but with the closest solvation shell compressed inward by a full 0.5 Å or half an O−H bond length.

We can better understand how the solvation structure of the hydrated electron in the optimized TBSE+OptPol model relates to that of the original TB model by considering the number of waters in the first solvation shell around the electron, n, which we take to be the number of water oxygens between the electron's center of mass and the first minimum of the electron-oxygen radial distribution function (3.3 and 3.7 Å for TBSE+OptPol and original TB, respectively). With this definition, the TBSE+OptPol and original TB hydrated electrons have similar coordination numbers of $n = 4.89 \pm 0.02$ and $n = 4.59 \pm 0.03$, respectively. Thus, reinforcing our conclusions from Figure 8, the effect of the extra attraction in the optimized polarization potential is, on average, to compress inward the four-to-five first-solvation-shell waters of the original TB model by roughly half the O−H bond length, resulting in a

negligible or at least vanishingly small cavity at the center of the hydrated electron's charge distribution. Indeed, the TBSE +OptPol electron has a nonzero probability to find a water H atom at the electron's center of mass, as illustrated in the TOC graphic.

Since the spatial extent of a hydrated electron is several Angstroms across, as indicated by a cross-section of the electron density in Figure 7 (solid red curves), the negligibly small cavity seen in the TBSE+OptPol model means that, on average, a substantial number of water molecules are within the charge density of the electron. If we define the radial extent of the electron as 3.25 Å, then the average number of water molecules inside the excess electron's charge density is 4.68 ± 0.04, corresponding to an average interior water density of D_{INT} = 0.973 ± 0.009 g cm^{-3}, which is just 3% lower than pure water. This can be compared to the values for the original TB model and the LGS noncavity model of D_{INT} = 0.541 ± 0.009 g cm^{-3} and 1.42 ± 0.01 g cm^{-3}, respectively. Clearly, the new TBSE+OptPol potential has a substantial increase in the overall attraction between the electron and water at short-range compared to the TB model. However, the TBSE+OptPol potential is not as attractive as the (known to be overly attractive) LGS model, which exhibits an interior water density above the bulk value.

All of this suggests that, unlike the large negative molar solvation volume of LGS,[15] the solvation volume of the TBSE +OptPol electron will be modest in magnitude.[53] Indeed, from the interfacial calculations described below in Section 3.3.4, we find that the change in volume (calculated following the procedure of ref 15) on adding an electron is consistent with a TBSE+OptPol molar solvation volume of −14 ± 12 cm^3 mol^{-1}. This value is in reasonable agreement with early experimental work that inferred a solvation volume of −1.7–2.7 cm^3 mol^{-1} from the variation of the rate constant of the electron's reactions with other species of known solvation volumes. However, a more recent time-resolved photoacoustic study yielded a solvation volume of +26 cm^3 mol^{-1}, consistent with the TB value of +31 ± 12 cm^3 mol^{-1}.[15] Based on this single observable, it thus appears that TBSE+OptPol may slightly overestimate the amount of electrostriction caused by the electron; however, given the fairly wide range in experimental values for the solvation volume of the electron, we believe that additional experiments would be useful in determining this quantity with higher accuracy.

Although it is clear that there is a greater degree of electron-water overlap in the TBSE+OptPol model compared to the TB model, the above discussion considers only the radial overlap. A better measure of electron-water overlap is found in the direct overlap[10]

$$\Theta = \left\langle \int \rho(\mathbf{r}) f(\mathbf{r}; \mathbf{R}^N) d\mathbf{r} \right\rangle$$

$$f(\mathbf{r}; \mathbf{R}^N) = \begin{cases} 1 \text{ for } |\mathbf{r} - \mathbf{R}_{COM,i}| < 1.0 \text{ Å, for any } i \\ 0 \text{ otherwise} \end{cases} \quad (9)$$

where $\rho(\mathbf{r})$ is the electron density, $f(\mathbf{r};\mathbf{R}^N)$ takes the value of 1 within 1 Å of any water molecule's center of mass, and $\mathbf{R}_{COM,i}$ and the angled brackets represent an ensemble average. This distance was chosen to correspond roughly with the radial extent of the oxygen core atomic orbitals. With this measure of electron-water overlap, we computed the TBSE+OptPol value of Θ to be 7.20 ± 0.04%, which is roughly midway between the

original TB value, 2.66 ± 0.02%, and the LGS value, 14.8 ± 0.2%.[54] Thus, consistent with the radial overlap, the new TBSE +OptPol model appears to have a structure that is intermediate between the cavity-forming TB model and the noncavity LGS model.

3.3.2. Vertical Binding Energy. Having explored the physical structure of the TBSE+OptPol hydrated electron, we consider now its electronic structure. Of direct relevance to experiment is the vertical binding energy, defined in Section 3.1. From our MQC MD simulations we computed a mean VBE of 3.62 ± 0.01 eV for the TBSE+OptPol model. This compares very favorably to experimental values, which range from 3.3 to 3.6 eV.[55−57] With our chosen simulation parameters, we find that the original TB model has a VBE of 2.69 ± 0.01 eV, which is somewhat lower than the value reported originally by TB, likely the result of our smaller simulation cell and the sensitivity of the VBE to truncation of the electron-water interaction. Thus, it is likely our predicted VBE for the TBSE+OptPol model is somewhat underestimated due to finite-size effects, and the converged value would thus be slightly higher in energy than the experimental value; but, as we have argued before,[7] we do not believe that a disagreement in the VBE necessarily invalidates the model, since the absolute value of the VBE is very sensitive to subtle details of the electron-water interaction at long-range.

Given this sensitivity of the VBE to the details of the potential, it is perhaps more instructive to analyze the relative magnitude of contributions to the VBE. Decomposing the VBE into contributions from the mean-field and polarization potentials, we find that the polarization-correlation energy (i.e., the expectation value of the polarization potential) of TBSE+OptPol is −2.356 ± 0.009 eV, which makes up more than half of the total binding energy. In contrast, the polarization-correlation energy of the original TB model is −0.930 ± 0.003 eV. Therefore, the ~0.9 eV increase in the electron binding energy in the TBSE+OptPol model from the original TB model comes largely from a ~1.4 eV increase in the polarization-correlation energy that is partially compensated by a ~0.5 eV reduction in the mean-field binding energy because of the larger Pauli repulsion between the electron and water molecules. Encouragingly, the mean polarization-correlation energy of the closest water molecule in the TBSE+OptPol model is −0.2877 ± 0.0009 eV, consistent with the magnitude of the correlation energy for the closest electron-water distances from the quantum chemistry calculations of Section 3.1. Furthermore, the closest 10 water molecules to the electron contribute, in total, a polarization-correlation energy of −1.378 ± 0.001 eV and −0.331 ± 0.001 eV in the TBSE+OptPol and TB models, respectively, meaning that the majority of the increased correlation energy in the TBSE+OptPol model is very short ranged and arises almost entirely from the first and second solvation-shell waters.

3.3.3. Optical Absorption Spectrum. The absorption spectrum is another observable of the hydrated electron's electronic structure that can be compared directly to experiment. We calculated the absorption spectrum of the hydrated electron for both the TB and TB+OptPol hydrated electrons in the inhomogeneous broadening limit

$$I(E) = \left\langle \sum_{i=1}^{N^{st}} |\mu_{0,i}|^2 \Delta E_{0,i} \delta(E - \Delta E_{0,i}) \right\rangle \quad (10)$$

where $\mu_{0,i}$ is the transition dipole moment between the ground state, 0, and state i, and $\Delta E_{0,i}$ is the excitation energy for state i, and we included $N^{st} = 19$ excited states.

For a finite-length simulation run, eq 10 gives a set of stick spectra, so in order to generate a continuous spectrum with which to compare to experiment we convolved eq 10 with a Gaussian kernel with exponent $\alpha = 50$ eV^{-2}. The resulting spectra for the TB and TBSE+OptPol models are shown in Figure 9(a) as the dashed red and solid black curves, respectively.
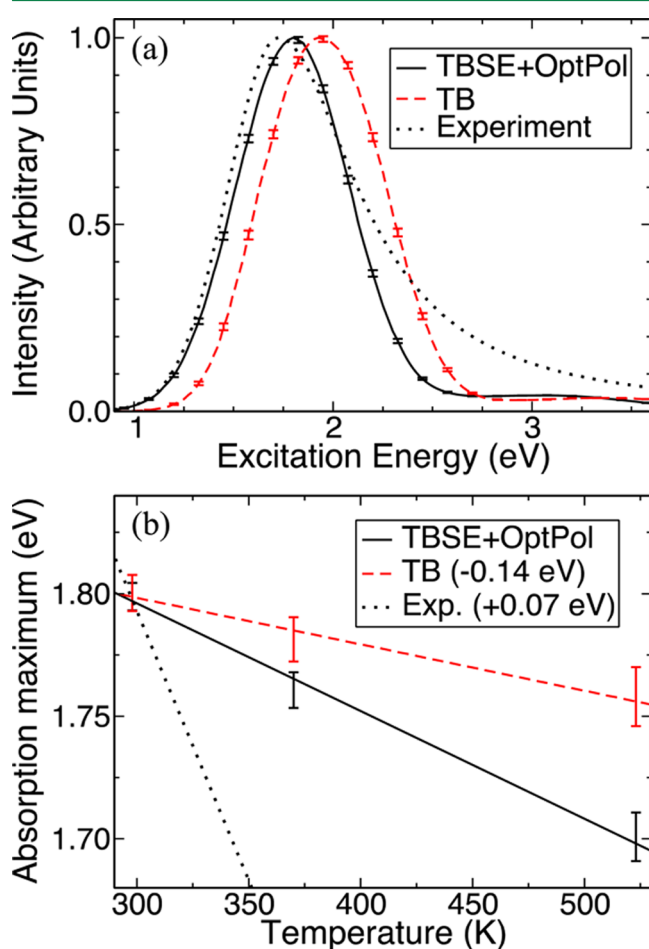

Figure 9. Optical absorption spectrum of the hydrated electron. Panel (a) shows the absorption spectra computed from the TBSE+OptPol (solid black curve) and TB models (dashed red curve), normalized to their absorption maxima. Both spectra are similar in shape, but compared to TB, the TBSE+OptPol model has an absorption maximum energy in better agreement with experiment (dotted black curve, which is a Gaussian−Lorentzian fit from ref 58). Panel (b) shows the temperature dependence of the maximum absorption energy: experiment (dotted black curve, from ref 59) shows a temperature dependence that is larger than either model, but the TBSE+OptPol model is again in better agreement with experiment compared to the TB model.

The figure shows that both models are in generally good agreement with the experimental spectrum (dotted black curve) but that the noncavity TBSE+OptPol model is in better agreement with experiment than TB based on the peak absorption energy. Both models underestimate the magnitude of the blue absorption tail, which is likely the result of neglecting self-consistent polarization.[60,61]

That the absorption spectrum in the noncavity TBSE+OptPol model is largely consistent with experiment is encouraging; however, our experience suggests that all this really indicates is that the model correctly predicts the size (radius of gyration) of the hydrated electron. Indeed, the radius of gyration of the electron can be found directly from the absorption spectrum by moment analysis, so the absorption spectrum is not all that sensitive a probe of the electronic or solvation structure. The TB and TBSE+OptPol models give radii of gyration of $\langle r^2 \rangle^{1/2} = 2.388 \pm 0.003$ Å and 2.480 ± 0.002 Å, respectively, both in excellent agreement with the experimental moment analysis value of 2.48 Å.[58]

Because of the relative insensitivity of the absorption spectrum to the underlying structure, we have proposed previously that a better experimental indicator of the hydrated electron's structure is the temperature dependence of the absorption spectrum.[13] Previous simulations of cavity models of the hydrated electron predicted that there is little noticeable dependence of the absorption spectrum with temperature. This result is in disagreement with experiment, which shows a substantial red-shift of the absorption with increasing temperature. The noncavity LGS hydrated electron model also shows a substantial red-shift of the absorption spectrum with increasing temperature, although the slope of the T dependence is about twice that seen experimentally.[16] Following the arguments of WCA theory,[62] the noncavity TBSE+OptPol model, with its more attractive electron-water interactions due to electron correlation, might be expected to show larger variations of its properties with temperature, particularly compared to the cavity TB model that, at short-range, is dominated almost exclusively by repulsive interactions.[7]

To test the temperature dependence of the TBSE+OptPol model, we simulated the hydrated electron at two additional temperatures, $T = 370$ and 523 K, and computed the absorption maximum energy, E^{MAX}, at each. Previous approaches to extracting the absorption maximum energy involved first histogramming eq 10 then fitting to an analytical form.[16] We found that such an approach was too sensitive to the choice of histogram bin width and fitting function to extract small temperature dependences of the absorption spectra. Instead, as described in the Appendix, we developed an approach to compute directly the absorption maximum energy from the MQC simulations, the temperature dependence of which is shown in Figure 9(b).

From weighted-least-squares fitting of the data in Figure 9(b) to a straight line, we find that the rate of change of the TBSE+OptPol model's absorption maximum is $-(4.4 \pm 0.5) \times 10^{-4}$ eV/K while that of the TB model is $-(1.9 \pm 0.6) \times 10^{-4}$ eV/K. Thus, we find that both models show only a slight redshift of the absorption spectrum with increasing temperature, with the TBSE+OptPol model shifting at roughly twice the rate as TB. These values can be compared to the experimental temperature-dependent shift of -2.2×10^{-3} eV/K. Thus, although both models substantially underestimate the temperature dependence of the absorption spectrum, it is encouraging that the TBSE+OptPol model has a more than 2-fold improvement over the original TB model.

3.3.4. Surface Activity of the Hydrated Electron. Although the noncavity TBSE+OptPol model shows improved agreement with experiment for the optical absorption spectrum and its temperature dependence compared to the cavity TB model, the improvements are fairly modest, and it could be argued that for the observables considered thus far, both models do about

as well as each other at predicting the experimental properties of the hydrated electron. We thus seek an experimental observable to better distinguish the cavity TB and noncavity TBSE+OptPol model. As we have argued recently,[15] the surface activity of the hydrated electron might be one such observable, with the TB cavity model predicting that the electron is (quasi)-stable at the air/water interface while the LGS noncavity electron is strongly repelled from the interface, favoring bulk solvation.

To understand the surface activity of the TBSE+OptPol model, we generated the Potential of Mean Force (PMF) for the electron relative to the instantaneous air/water interface, using the Quantum Biased Molecular Dynamics method and other simulation details as described in ref 15. The results are shown in Figure 10(a), where we see that, similar to the
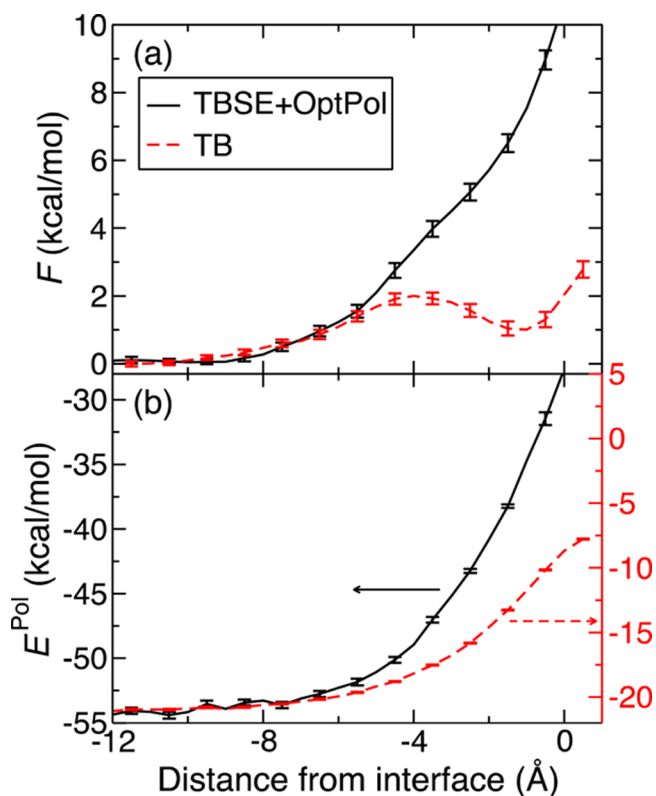

Figure 10. Panel (a): the PMF (i.e., Gibbs free energy) for noncavity TBSE+OptPol (black solid curve) and cavity TB (dashed red curve) hydrated electrons as a function of vertical distance from the instantaneous air/water interface. Negative distances indicate displacements below the interface. Panel (b): the mean electron-water polarization energy as a function of distance from the instantaneous air/water interface for the TBSE+OptPol (black solid curve, left axis) and cavity TB (dashed red curve, right axis) models. The TBSE +OptPol electron is repelled from the interface more than the TB electron due to the stronger electron-water polarization potential in the former that favors bulk solvation.

noncavity LGS model,[15] the TBSE+OptPol electron (solid black curve) is repelled by the air/water interface, whereas the TB electron (dashed red curve) has a local minimum at the interface. This behavior can be understood from the variation of the mean polarization energy (expectation value of the polarization potential of eq 6) with distance from the interface, plotted in Figure 10(b): in both models, the polarization potential (which captures electron-water polarization and

correlation) favors solvation in the bulk, which makes sense as this interaction scales with increasing water density. However, the polarization potential is significantly larger in magnitude in TBSE+OptPol compared to TB. This is why the TBSE+OptPol model is more strongly stabilized by bulk water compared to interfacial solvation.

Several experiments have been carried out to address whether or not the hydrated electron prefers to localize at the air/water interface, but as of yet there does not appear to be a consensus. For example, one time-resolved photoelectron spectroscopy experiment in liquid microjet found a stable peak for the hydrated electron at ~1.6 eV binding energy, suggestive of a stable surface-localized electron,[55] but this result has not been reproduced by a number of other groups.[57,63−65] Second harmonic generation (SHG) experiments by Verlet and co-workers strongly suggest that the electron can reside within ~1 nm of the interface;[66] however, we have argued previously that electrons as close as 0.6 nm to the interface are effectively bulk electrons and not interfacial electrons.[15] A more recent sum-frequency generation (SFG) study by Tahara and co-workers, in contrast, provides indirect evidence based on changes in water's vibrational spectrum that electrons generated near the interface may in fact remain there for ~10 ps.[67] It is clear that further theoretical and experimental work is needed to understand the surface activity of the hydrated electron. The results presented in Figure 10 motivate this by showing that the surface activity of the hydrated electron is a useful experimental observable that should distinguish cavity from noncavity solvation and that proper treatment of short-range correlation can change the electron's interfacial behavior.

To summarize, in Table 1 we collect the range of computed observables for both the original TB model and the TBSE model with our optimized polarization term. We find that the TBSE+OptPol model of the hydrated electron shows noncavity behavior, with a structure and properties that are intermediate between the cavity TB model and the noncavity LGS model. The observables of TBSE+OptPol are all in better agreement with experiment compared to TB although the improvements are fairly modest in magnitude, suggesting there is still room for additional progress. Indeed, in the Supporting Information, we also present the calculated resonance Raman spectrum of the TBSE+OptPol hydrated electron; we find that the Raman spectrum is largely unchanged from that of the TB model, which is substantially blue-shifted and narrowed compared to experiment.

4. CONCLUSIONS

Overall, our results suggest that electron correlation may be one of the most important factors in determining the structure of the hydrated electron. Although it may seem surprising that the importance of electron correlation interactions to the bulk hydrated electron's structure has been overlooked up to this point, previous quantum chemical explorations of electron-water dispersion interactions have been confined to either 1) small-to-moderate-sized water anion clusters, where the electron's diffuseness and large average distance from the water molecules is not representative of the condensed phase or 2) to model cavity structures that also presuppose a separation of the electron and water by several angstroms. Indeed, we find that when an excess electron is confined to be directly on a water molecule, the per water electron correlation interactions are an order of magnitude larger than those typically found in small cluster anions. As a result, electron-water models

Table 1. Properties of the Hydrated Electron from Cavity and Noncavity Models

property[a]	TB (cavity)	LGS (noncavity)	TBSE+OptPol (noncavity)	experiment
D_{INT} (g/cm^3)[b]	0.541 ± 0.009	1.42 ± 0.01	0.973 ± 0.009	
Θ[c]	$2.66 \pm 0.02\%$	$14.8 \pm 0.2\%$	$7.20 \pm 0.04\%$	
VBE (eV)[d]	2.69 ± 0.01	5.19 ± 0.07	3.62 ± 0.01	$3.3-3.6$[j]
$\langle r^2 \rangle^{1/2}$ (Å)	2.388 ± 0.003	2.46 ± 0.04	2.480 ± 0.002	2.48[k]
E^{MAX} (eV)[e]	1.940 ± 0.007	1.71 ± 0.06	1.799 ± 0.006	1.728[k]
dE^{MAX}/dT (eV/K)[f]	$-(1.9 \pm 0.6) \times 10^{-4}$	-5.2×10^{-3}[i]	$-(4.4 \pm 0.5) \times 10^{-4}$	-2.2×10^{-3}[l]
V (cm^3/mol)[g]	$+31 \pm 12$[h]	-116 ± 27[h]	-14 ± 12	$-1.7-2.7$[m], $+26$[n]

[a]Evaluated at 298 K and density 0.9970479 g cm^{-3}. [b]Interior water density, corresponding to the average water density within 3.25 Å of the electron center of mass. [c]Electron-water direct overlap (see eq 9). [d]Vertical Binding Energy. [e]Optical absorption spectrum peak position. [f]Linear temperature dependence of spectral peak position. [g]Partial Molar Volume. [h]Taken from ref 15. [i]Reference 16. [j]References 55−57. [k]Reference 58. [l]Reference 59. [m]Reference 68. [n]Reference 53.

parametrized to fit cluster energetics[22−24,29,31,69] may not be transferable to the condensed phase since the short-range part of the electron correlation interaction is poorly sampled.

To remedy this poor treatment of electron correlation interactions at short distances, we developed a confining-potential approach to allow a high-level quantum chemical determination of electron-water interactions over a range of electron-water displacements. We found that at short-range, electron correlation interactions are surprisingly large, being comparable in magnitude to the mean-field Hartree−Fock electron-water interactions. Furthermore, our results show that Hartree−Fock theory provides an inadequate description of electron-water interactions and that a fully *ab initio* description of the hydrated electron requires at least the MP2 level of theory and preferably CCSD(T). Although DFT might provide a computationally cheaper alternative, the ability of modern functionals to correctly describe both short-range and long-range (dispersion) electron-water correlation interactions remains to be determined.

By analyzing Pair Correlation Energies between the electron and water, we found that the strength of the electron correlation interaction results from the large overlap of the excess electron's SOMO and occupied water orbitals. When we then fit a model one-electron potential to the distance-dependent CCSD(T) electron-water interactions, we showed that the short-range correlation interactions are sufficiently attractive to stabilize noncavity solvation motifs of the hydrated electron, where water molecules are able to penetrate to the center of the excess electron's charge density, even when a strongly cavity-forming static exchange core potential is used. The properties of the hydrated electron computed with our new potential show better agreement with experiment compared to the original cavity TB model, although there is still clearly room for improvement. Nevertheless, our results strongly suggest that no matter what the details of the core potential,[7−9] a proper treatment of electron correlation interactions is sufficient to drive a noncavity solvation structure for the hydrated electron.

■ APPENDIX

Here we present our method for computing an absorption spectrum maximum directly from mixed quantum/classical simulations. As described in Section 3.3.3, the starting point is the expression for the absorption spectrum in the inhomogeneous broadening limit, eq 10. After convolving with a Gaussian kernel, this expression becomes

$$I^{sm}(E) = \left\langle \sum_{i=1}^{N^{st}} |\mu_{0,i}|^2 \Delta E_{0,i} \sqrt{\alpha/\pi} \, \exp(-\alpha(E - \Delta E_{0,i})^2) \right\rangle \tag{11}$$

We found that a smoothing parameter of $\alpha = 50$ eV^{-2} gave a faithful representation of the hydrated electron's spectrum while sufficiently smoothing out statistical noise. The absorption spectrum maximum was then found from the extremum condition

$$\left. \frac{dI^{sm}}{dE} \right|_{E^{max}} = 0$$

$$\sum_{J=1}^{N^{snap}} \sum_{i=1}^{N^{st}} -|\mu_{0,i}^J|^2 \Delta E_{0,i}^J (E^{max} - \Delta E_{0,i}^J) \exp(-\alpha(E^{max} - \Delta E_{0,i}^J)^2) = 0 \tag{12}$$

where the second equality results from rewriting the ensemble average as a sum over N^{snap} simulation snapshots, and $\mu_{0,i}^J$ and $\Delta E_{0,i}^J$ are respectively the transition dipole and transition energy of state i for snapshot J. Given its analytical form, eq 12 was readily solved with the Newton−Raphson method. Finally, the standard error in the absorption maximum energy was determined by linearizing eq 12 around E^{max}:

$$\delta E^{max} = \delta \left(\left. \frac{dI^{sm}}{dE} \right|_{E^{max}} \right) \times \left(\left. \frac{-d^2 I^{sm}}{dE^2} \right|_{E^{max}} \right)^{-1} \tag{13}$$

The advantage of this approach, compared to first generating a spectrum by histogramming eq 10 and then fitting to an analytical form,[16] is that the computed absorption spectrum maximum in our approach does not depend on the choice of histogram bin width or fitting function, both of which we found to be quite sensitive in determining the position of the spectral maximum.

■ ASSOCIATED CONTENT

ⓢ Supporting Information

The Supporting Information is available free of charge on the ACS Publications website at DOI: 10.1021/acs.jctc.6b00472.

Computed resonance Raman spectra for the TBSE +OptPol model of the hydrated electron (PDF)

■ AUTHOR INFORMATION

Corresponding Authors
*E-mail: william.glover@nyu.edu.
*E-mail: schwartz@chem.ucla.edu.

■ REFERENCES

(1) Rossky, P. J.; Schnitker, J. The Hydrated Electron: Quantum Simulation of Structure, Spectroscopy, and Dynamics. *J. Phys. Chem.* **1988**, *92*, 4277.

(2) Turi, L.; Borgis, D. Analytical Investigations of an Electron-Water Molecule Pseudopotential. II. Development of a New Pair Potential and Molecular Dynamics Simulations. *J. Chem. Phys.* **2002**, *117*, 6186.

(3) Kevan, L. Solvated Electron Structure in Glassy Matrixes. *Acc. Chem. Res.* **1981**, *14*, 138.

(4) Soper, A. K.; Weckström, K. Ion Solvation and Water Structure in Potassium Halide Aqueous Solutions. *Biophys. Chem.* **2006**, *124*, 180.

(5) Smith, J. D.; Saykally, R. J.; Geissler, P. L. The Effects of Dissolved Halide Anions on Hydrogen Bonding in Liquid Water. *J. Am. Chem. Soc.* **2007**, *129*, 13847.

(6) Larsen, R. E.; Glover, W. J.; Schwartz, B. J. Does the Hydrated Electron Occupy a Cavity? *Science* **2010**, *329*, 65.

(7) Larsen, R. E.; Glover, W. J.; Schwartz, B. J. Response to Comments on "Does the Hydrated Electron Occupy a Cavity?". *Science* **2011**, *331*, 1387.

(8) Jacobson, L. D.; Herbert, J. M. Comment on "Does the Hydrated Electron Occupy a Cavity?". *Science* **2011**, *331*, 1387.

(9) Turi, L.; Madarász, Á. Comment on "Does the Hydrated Electron Occupy a Cavity?". *Science* **2011**, *331*, 1387.

(10) Casey, J. R.; Kahros, A.; Schwartz, B. J. To Be or Not to Be in a Cavity: The Hydrated Electron Dilemma. *J. Phys. Chem. B* **2013**, *117*, 14173.

(11) Uhlig, F.; Marsalek, O.; Jungwirth, P. Unraveling the Complex Nature of the Hydrated Electron. *J. Phys. Chem. Lett.* **2012**, *3*, 3071.

(12) Kumar, A.; Walker, J. A.; Bartels, D. M.; Sevilla, M. D. A Simple ab Initio Model for the Hydrated Electron That Matches Experiment. *J. Phys. Chem. A* **2015**, *119*, 9148.

(13) Turi, L. Hydrated Electrons in Water Clusters: Inside or Outside, Cavity or Noncavity? *J. Chem. Theory Comput.* **2015**, *11*, 1745.

(14) Turi, L. On the Applicability of One- and Many-Electron Quantum Chemistry Models for Hydrated Electron Clusters. *J. Chem. Phys.* **2016**, *144*, 154311.

(15) Casey, J. R.; Schwartz, B. J.; Glover, W. J. Free Energies of Cavity and Noncavity Hydrated Electrons Near the Instantaneous Air/Water Interface. *J. Phys. Chem. Lett.* **2016**, *7*, 3192.

(16) Casey, J. R.; Larsen, R. E.; Schwartz, B. J. Resonance Raman and Temperature-Dependent Electronic Absorption Spectra of Cavity and Noncavity Models of the Hydrated Electron. *Proc. Natl. Acad. Sci. U. S. A.* **2013**, *110*, 2712.

(17) Schnitker, J.; Rossky, P. J. Quantum Simulation Study of the Hydrated Electron. *J. Chem. Phys.* **1987**, *86*, 3471.

(18) Schnitker, J.; Rossky, P. J. An Electron−Water Pseudopotential for Condensed Phase Simulation. *J. Chem. Phys.* **1987**, *86*, 3462.

(19) Barnett, R. N.; Landman, U.; Cleveland, C. L.; Jortner, J. Electron Localization in Water Clusters. II. Surface and Internal States. *J. Chem. Phys.* **1988**, *88*, 4429.

(20) Turi, L.; Gaigeot, M. P.; Levy, N.; Borgis, D. Analytical Investigations of an Electron−Water Molecule Pseudopotential. I. Exact Calculations on a Model System. *J. Chem. Phys.* **2001**, *114*, 7805.

(21) Madarász, Á.; Rossky, P. J.; Turi, L. Excess Electron Relaxation Dynamics at Water/Air Interfaces. *J. Chem. Phys.* **2007**, *126*, 234707.

(22) Sommerfeld, T.; DeFusco, A.; Jordan, K. D. Model Potential Approaches for Describing the Interaction of Excess Electrons with Water Clusters: Incorporating Long-Range Correlation Effects. *J. Phys. Chem. A* **2008**, *112*, 11021.

(23) Jacobson, L. D.; Williams, C. F.; Herbert, J. M. The Static-Exchange Electron-Water Pseudopotential, in Conjunction with a Polarizable Water Model: A New Hamiltonian for Hydrated-Electron Simulations. *J. Chem. Phys.* **2009**, *130*, 124115.

(24) Jacobson, L. D.; Herbert, J. M. A One-Electron Model for the Aqueous Electron that Includes Many-Body Electron-Water Polarization: Bulk Equilibrium Structure, Vertical Electron Binding Energy, and Optical Absorption Spectrum. *J. Chem. Phys.* **2010**, *133*, 154506.

(25) Herbert, J. M.; Jacobson, L. D. Structure of the Aqueous Electron: Assessment of One-Electron Pseudopotential Models in Comparison to Experimental Data and Time-Dependent Density Functional Theory. *J. Phys. Chem. A* **2011**, *115*, 14470.

(26) Smallwood, C. J.; Larsen, R. E.; Glover, W. J.; Schwartz, B. J. A Computationally Efficient Exact Pseudopotential Method. I. Analytic Reformulation of the Phillips-Kleinman Theory. *J. Chem. Phys.* **2006**, *125*, 074102.

(27) Williams, C. F.; Herbert, J. M. Influence of Structure on Electron Correlation Effects and Electron−Water Dispersion Interactions in Anionic Water Clusters. *J. Phys. Chem. A* **2008**, *112*, 6171.

(28) Wang, F.; Jordan, K. D. Application of a Drude Model to the Binding of Excess Electrons to Water Clusters. *J. Chem. Phys.* **2002**, *116*, 6973.

(29) Sommerfeld, T.; Jordan, K. D. Quantum Drude Oscillator Model for Describing the Interaction of Excess Electrons with Water Clusters: An Application to (H2O)13-. *J. Phys. Chem. A* **2005**, *109*, 11531.

(30) Herbert, J. M.; Head-Gordon, M. Accuracy and Limitations of Second-Order Many-Body Perturbation Theory for Predicting Vertical Detachment Energies of Solvated-Electron Clusters. *Phys. Chem. Chem. Phys.* **2006**, *8*, 68.

(31) Sommerfeld, T.; Jordan, K. D. Electron Binding Motifs of (H2O)n- Clusters. *J. Am. Chem. Soc.* **2006**, *128*, 5828.

(32) Voora, V. K.; Ding, J.; Sommerfeld, T.; Jordan, K. D. A Self-Consistent Polarization Potential Model for Describing Excess Electrons Interacting with Water Clusters. *J. Phys. Chem. B* **2013**, *117*, 4365.

(33) Møller, C.; Plesset, M. S. Note on an Approximation Treatment for Many-Electron Systems. *Phys. Rev.* **1934**, *46*, 618.

(34) Pople, J. A.; Head-Gordon, M.; Raghavachari, K. Quadratic Configuration Interaction. A General Technique for Determining Electron Correlation Energies. *J. Chem. Phys.* **1987**, *87*, 5968.

(35) Taken from Figure 2A of ref 6.

(36) NIST Computational Chemistry Comparison and Benchmark Database. http://cccbdb.nist.gov/ (accessed July 1, 2016).

(37) Shao, Y.; Gan, Z.; Epifanovsky, E.; Gilbert, A. T. B.; Wormit, M.; Kussmann, J.; Lange, A. W.; Behn, A.; Deng, J.; Feng, X.; Ghosh, D.; Goldey, M.; Horn, P. R.; Jacobson, L. D.; Kaliman, I.; Khaliullin, R. Z.; Kuś, T.; Landau, A.; Liu, J.; Proynov, E. I.; Rhee, Y. M.; Richard, R. M.; Rohrdanz, M. A.; Steele, R. P.; Sundstrom, E. J.; Woodcock, H. L.; Zimmerman, P. M.; Zuev, D.; Albrecht, B.; Alguire, E.; Austin, B.; Beran, G. J. O.; Bernard, Y. A.; Berquist, E.; Brandhorst, K.; Bravaya, K. B.; Brown, S. T.; Casanova, D.; Chang, C.-M.; Chen, Y.; Chien, S. H.; Closser, K. D.; Crittenden, D. L.; Diedenhofen, M.; DiStasio, R. A.; Do, H.; Dutoi, A. D.; Edgar, R. G.; Fatehi, S.; Fusti-Molnar, L.; Ghysels, A.; Golubeva-Zadorozhnaya, A.; Gomes, J.; Hanson-Heine, M. W. D.; Harbach, P. H. P.; Hauser, A. W.; Hohenstein, E. G.; Holden, Z. C.; Jagau, T.-C.; Ji, H.; Kaduk, B.; Khistyaev, K.; Kim, J.; Kim, J.; King, R. A.; Klunzinger, P.; Kosenkov, D.; Kowalczyk, T.; Krauter, C. M.; Lao, K. U.; Laurent, A. D.; Lawler, K. V.; Levchenko, S. V.; Lin, C. Y.; Liu, F.; Livshits, E.; Lochan, R. C.; Luenser, A.; Manohar, P.; Manzer, S. F.; Mao, S.-P.; Mardirossian, N.; Marenich, A. V.; Maurer, S. A.; Mayhall, N. J.; Neuscamman, E.; Oana, C. M.; Olivares-Amaya, R.; O'Neill, D. P.; Parkhill, J. A.; Perrine, T. M.; Peverati, R.; Prociuk, A.; Rehn, D. R.; Rosta, E.; Russ, N. J.; Sharada, S. M.; Sharma, S.; Small, D. W.; Sodt, A.; Stein, T.; Stück, D.; Su, Y.-C.;

Thom, A. J. W.; Tsuchimochi, T.; Vanovschi, V.; Vogt, L.; Vydrov, O.; Wang, T.; Watson, M. A.; Wenzel, J.; White, A.; Williams, C. F.; Yang, J.; Yeganeh, S.; Yost, S. R.; You, Z.-Q.; Zhang, I. Y.; Zhang, X.; Zhao, Y.; Brooks, B. R.; Chan, G. K. L.; Chipman, D. M.; Cramer, C. J.; Goddard, W. A.; Gordon, M. S.; Hehre, W. J.; Klamt, A.; Schaefer, H. F.; Schmidt, M. W.; Sherrill, C. D.; Truhlar, D. G.; Warshel, A.; Xu, X.; Aspuru-Guzik, A.; Baer, R.; Bell, A. T.; Besley, N. A.; Chai, J.-D.; Dreuw, A.; Dunietz, B. D.; Furlani, T. R.; Gwaltney, S. R.; Hsu, C.-P.; Jung, Y.; Kong, J.; Lambrecht, D. S.; Liang, W.; Ochsenfeld, C.; Rassolov, V. A.; Slipchenko, L. V.; Subotnik, J. E.; Van Voorhis, T.; Herbert, J. M.; Krylov, A. I.; Gill, P. M. W.; Head-Gordon, M. Advances in Molecular Quantum Chemistry Contained in the Q-Chem 4 Program Package. *Mol. Phys.* **2015**, *113*, 184.

(38) Szabo, A.; Ostlund, N. S. *Modern Quantum Chemistry: Introduction to Advanced Electronic Structure Theory*; Dover Publications: 1989; pp 124−128.

(39) Gutowski, M.; Skurski, P. Dispersion Stabilization of Solvated Electrons and Dipole-Bound Anions. *J. Phys. Chem. B* **1997**, *101*, 9143.

(40) Turney, J. M.; Simmonett, A. C.; Parrish, R. M.; Hohenstein, E. G.; Evangelista, F. A.; Fermann, J. T.; Mintz, B. J.; Burns, L. A.; Wilke, J. J.; Abrams, M. L.; Russ, N. J.; Leininger, M. L.; Janssen, C. L.; Seidl, E. T.; Allen, W. D.; Schaefer, H. F.; King, R. A.; Valeev, E. F.; Sherrill, C. D.; Crawford, T. D. Psi4: an Open-Source Ab Initio Electronic Structure Program. *WIREs Comput. Mol. Sci.* **2012**, *2*, 556.

(41) Davidson, E. R. The Iterative Calculation of a Few of the Lowest Eigenvalues and Corresponding Eigenvectors of Large Real-Symmetric Matrices. *J. Comput. Phys.* **1975**, *17*, 87.

(42) Szász, L. *Pseudopotential Theory of Atoms and Molecules*; J. Wiley: 1985.

(43) Stampfli, P. Theory for the Electron Affinity of Clusters of Rare Gas Atoms and Polar Molecules. *Phys. Rep.* **1995**, *255*, 1.

(44) Simons, J. One-Electron Electron−Molecule Potentials Consistent with ab Initio Møller−Plesset Theory. *J. Phys. Chem. A* **2010**, *114*, 8631.

(45) We explored a variety of other short-range damping functions but found the functional form of the TB polarization potential gave the best fit.

(46) Marquardt, D. W. An Algorithm for Least-Squares Estimation of Nonlinear Parameters. *J. Soc. Ind. Appl. Math.* **1963**, *11*, 431.

(47) Toukan, K.; Rahman, A. Molecular-Dynamics Study of Atomic Motions in Water. *Phys. Rev. B: Condens. Matter Mater. Phys.* **1985**, *31*, 2643.

(48) Bussi, G.; Donadio, D.; Parrinello, M. Canonical Sampling Through Velocity Rescaling. *J. Chem. Phys.* **2007**, *126*, 014101.

(49) Hellmann, H. *Einführung in die Quantenchemie*; F. Deuticke: Leipzig, 1937; p 285.

(50) Feynman, R. P. Forces in Molecules. *Phys. Rev.* **1939**, *56*, 340.

(51) Swope, W. C.; Andersen, H. C.; Berens, P. H.; Wilson, K. R. A Computer Simulation Method for the Calculation of Equilibrium Constants for the Formation of Physical Clusters of Molecules: Application to Small Water Clusters. *J. Chem. Phys.* **1982**, *76*, 637.

(52) Shirts, M. R.; Chodera, J. D. Statistically Optimal Analysis of Samples from Multiple Equilibrium States. *J. Chem. Phys.* **2008**, *129*, 124105.

(53) Borsarelli, C. D.; Bertolotti, S. G.; Previtali, C. M. Thermodynamic Changes Associated with the Formation of the Hydrated Electron after Photoionization of Inorganic Anions: a Time-Resolved Photoacoustic Study. *Photochem. Photobiol. Sci.* **2003**, *2*, 791.

(54) The computed values of electron-water direct overlap are slightly smaller than those published in ref 10. This is because the definition of direct overlap in ref 10 double counted electron density that fell within overlapping regions of two or more neighboring water molecules.

(55) Siefermann, K. R.; Liu, Y.; Lugovoy, E.; Link, O.; Faubel, M.; Buck, U.; Winter, B.; Abel, B. Binding Energies, Lifetimes and Implications of Bulk and Interface Solvated Electrons in Water. *Nat. Chem.* **2010**, *2*, 274.

(56) Tang, Y.; Shen, H.; Sekiguchi, K.; Kurahashi, N.; Mizuno, T.; Suzuki, Y.-I.; Suzuki, T. Direct Measurement of Vertical Binding Energy of a Hydrated Electron. *Phys. Chem. Chem. Phys.* **2010**, *12*, 3653.

(57) Shreve, A. T.; Yen, T. A.; Neumark, D. M. Photoelectron Spectroscopy of Hydrated Electrons. *Chem. Phys. Lett.* **2010**, *493*, 216.

(58) Bartels, D. M.; Takahashi, K.; Cline, J. A.; Marin, T. W.; Jonah, C. D. Pulse Radiolysis of Supercritical Water. 3. Spectrum and Thermodynamics of the Hydrated Electron. *J. Phys. Chem. A* **2005**, *109*, 1299.

(59) Du, Y.; Price, E.; Bartels, D. M. Solvated Electron Spectrum in Supercooled Water and Ice. *Chem. Phys. Lett.* **2007**, *438*, 234.

(60) Jacobson, L. D.; Herbert, J. M. Polarization-Bound Quasi-Continuum States Are Responsible for the "Blue Tail" in the Optical Absorption Spectrum of the Aqueous Electron. *J. Am. Chem. Soc.* **2010**, *132*, 10000.

(61) An additional consequence of the neglect of self-consistent polarization is that the TBSE+OptPol model overestimates the VBE of the bulk hydrated electron at 3.62 eV, which itself is likely an underestimate of the true value from the model due to the small simulation cell used. However, this is not necessarily cause for concern, because unlike structural properties, VBEs are very sensitive to long-range interactions.

(62) Andersen, H. C.; Chandler, D.; Weeks, J. D. Roles of Repulsive and Attractive Forces in Liquids: The Equilibrium Theory of Classical Fluids. *Adv. Chem. Phys.* **1976**, *34*, 105.

(63) Lubcke, A.; Buchner, F.; Heine, N.; Hertel, I. V.; Schultz, T. Time-Resolved Photoelectron Spectroscopy of Solvated Electrons in Aqueous NaI Solution. *Phys. Chem. Chem. Phys.* **2010**, *12*, 14629.

(64) Buchner, F.; Schultz, T.; Lubcke, A. Solvated Electrons at the Water-Air Interface: Surface Versus Bulk Signal in Low Kinetic Energy Photoelectron Spectroscopy. *Phys. Chem. Chem. Phys.* **2012**, *14*, 5837.

(65) Yamamoto, Y.-i.; Suzuki, Y.-I.; Tomasello, G.; Horio, T.; Karashima, S.; Mitríc, R.; Suzuki, T. Time- and Angle-Resolved Photoemission Spectroscopy of Hydrated Electrons Near a Liquid Water Surface. *Phys. Rev. Lett.* **2014**, *112*, 187603.

(66) Sagar, D. M.; Bain, C. D.; Verlet, J. R. R. Hydrated Electrons at the Water/Air Interface. *J. Am. Chem. Soc.* **2010**, *132*, 6917.

(67) Matsuzaki, K.; Kusaka, R.; Nihonyanagi, S.; Yamaguchi, S.; Nagata, T.; Tahara, T. Partially Hydrated Electrons at the Air/Water Interface Observed by UV-Excited Time-Resolved Heterodyne-Detected Vibrational Sum Frequency Generation Spectroscopy. *J. Am. Chem. Soc.* **2016**, *138*, 7551.

(68) Hentz, R. R.; Brazier, D. W. γ Radiolysis of Liquids at High Pressures. X. The Reaction H+OH− and the Partial Molal Volume of the Hydrated Electron. *J. Chem. Phys.* **1971**, *54*, 2777.

(69) Sommerfeld, T.; Gardner, S. D.; DeFusco, A.; Jordan, K. D. Low-lying Isomers and Finite Temperature Behavior of (H2O)6-. *J. Chem. Phys.* **2006**, *125*, 174301.